Published in *ASCE-ASME Journal of Risk and Uncertainty in Engineering Systems, Part B: Mechanical Engineering* 7 (4) **2021**

Impact of geotechnical uncertainty on the preliminary design of monopiles supporting offshore wind turbines

Cormac Reale[1,a], Jacques Tott-Buswell[2,b], Luke J Prendergast[2,c]*

[1] Centre for Infrastructure, Geotechnical and Water Engineering Research (IGWE),
Department of Architecture and Civil Engineering,
University of Bath,
Claverton Down,
Bath BA2 7AY,
United Kingdom

[2] Department of Civil Engineering,
Faculty of Engineering,
University of Nottingham,
Nottingham NG7 2RD,
United Kingdom

*Corresponding author

Email:
[a]cr760@bath.ac.uk,
[b]jacques.tott-buswell@nottingham.ac.uk,
[c]luke.prendergast@nottingham.ac.uk

Abstract:

The growing demand for clean renewable energy sources and the lack of suitable nearshore sites is moving the offshore wind industry toward developing larger wind turbines in deeper water locations further offshore. This is adding significant uncertainty to the geotechnical design of monopiles used as foundations for these systems. Soil testing becomes more challenging, rigid monopile behaviour is less certain, and design methods are being applied outside the bounds of the datasets from which they were originally derived. This paper examines the potential impact of certain elements of geotechnical uncertainty on monotonic load-displacement behaviour and design system natural frequency of an example monopile-supported offshore wind turbine (OWT). Geotechnical uncertainty is considered in terms of spatial variability in soil properties derived from Cone Penetration Tests (CPT), parameter

transformation uncertainty using the rigidity index, and design choice for subgrade reaction modelling. Results suggest that spatial variability in CPT properties exhibits limited impact on design load-displacement characteristics of monopiles as vertical spatial variability tends to be averaged out in the process to develop discrete soil reaction-lateral displacement (*p-y*) models. This highlights a potential issue whereby localised variations in soil properties may not be captured in certain models. Spatial variability in CPT data has a noticeable effect on predicted system frequency responses of OWTs employing a subgrade reaction model approach, and the influence of subgrade reaction model choice is significant. The purpose of this paper is to investigate the effect of uncertainty in soil data, model transformation, and design model choice on resulting structural behaviour for a subset of available design approaches. It should be noted that significant further uncertainty exists and a wide variety of alternative models can be used by designers, so the results should be interpreted qualitatively.

Keywords: Offshore wind; Natural frequency; Spatial variability; Geotechnical uncertainty; Monopiles

1.0 Introduction:

There is an increasing need for clean renewable energy production to sustain growing societal demand worldwide. The current over-reliance on fossil-fuels is having a detrimental effect on the World's climate and is leading to global energy security issues. The European Green Deal [1] sets out a goal of achieving a carbon neutral continent by 2050. Wind energy, which is seen as the most scientifically mature source of renewable energy, has risen to the challenge and realised significant growth in capability and production over recent years. By 2017, wind power already accounted for over 44% of all new power installations and supplied over 11% of Europe's electricity demand [2]. This is estimated to increase to over 30% by 2030. To date,

much of this progress has been accomplished by onshore wind installations, however there is growing opposition to the continued development of these farms due to aesthetic and environmental noise-related concerns. This has fuelled a move toward offshore wind as a more reliable and societally acceptable alternative.

The pace of offshore wind development has increased substantially in recent years with Europe remaining at the forefront of innovation in the area. Over 90% of current offshore wind turbines (OWTs) are located in European waters [2]. Policy support has enabled the European Union to reach over 20 GW of installed offshore capacity by 2018 [3]. Turbine technology has advanced considerably during this time, with both turbine sizes and power capacity/efficiency increasing. Since 2002, turbine heights have increased from an average of approximately 93 m to over 236 m predicted by 2022 [4]. These higher wind turbine towers require much larger foundations. In addition, many nearshore sites have already been exploited to date, so there is now a growing need to develop sites further offshore, which have less certain geotechnical properties and experience more severe wind and wave conditions.

Over 87% of OWTs developed to date are founded on single, large-diameter monopiles [2,5], which have typical diameters between 4 - 6m and embedded lengths in the range of 20 - 30 m [6,7]. As turbines grow in size, monopile diameters up to 10 m and beyond are planned, resulting in systems with very low slenderness (high rigidity), denoted as having a length/diameter (L/D) of 5 or below. Monopiles resist loads applied from wind and waves through rotation and developing flexural resistance, where the ultimate resistance is governed by the soil strength and pile geometrical properties. Monopiles are typically designed using a lateral resistance-displacement approach, namely the *p-y* method, which considers the pile as a beam supported by a nonlinear Winkler spring system [8–11]. The *p-y* behaviour is

characterised by load-displacement curves, and has been the subject of substantial research over recent years [5,12–15]. Monopiles are typically designed with a view to limiting mudline rotations to less than 0.25 degrees over the turbine lifespan [16]. As these systems become more rigid, the principles underlying the design become less certain, as current design approaches are based on experiments conducted on long, slender piles, which have very different load resistance characteristics [17–20].

In addition to static design, OWTs are dynamically-sensitive structures with strict requirements in terms of the system natural frequency. The rotation of blades and rotor imposes two excitations on the system, termed the 1P and 3P frequencies (for a standard three-bladed system) [6,21,22]. Monopile-supported systems are typically designed as soft-stiff, where the system frequency is designed to reside between these two operating excitation bands. For the avoidance of resonance, it is imperative that designers can accurately model the system to ensure these excitation frequencies do not overlap with the system natural frequency.

The rapid increase in turbine heights, larger monopile diameters, and the move to deeper-water far offshore locations where geotechnical conditions are less certain is leading to a perfect storm that risks stagnating the pace of development in the sector. The design of foundations under these conditions is at the operating limit of engineering experience to date, and confidence is lessening. There is growing concern over issues such as the accuracy of soil-structure interaction (SSI) coupling stiffness [23,24], the governing operating parameters [25], geotechnical parameter transformation [26], measurement uncertainty [27], influence of added mass [24,28], and the effects of model uncertainty [29,30]. These issues have the potential to undermine the pace of developments if not addressed.

This paper investigates the effect of certain types of geotechnical uncertainty on the load-displacement behaviour and design frequency of monopile-supported OWTs. A stochastic ground model based on CPT data is developed and the effects of model choice, parameter transformation and geotechnical uncertainty on the resulting behaviour of an example OWT are studied. The purpose of the study is to highlight how variability or uncertainty influences the predicted behaviour of an example OWT and a small set of available models and approaches are examined for this purpose. The study is not intended to inform users how to account for this variability, and it should be noted that there exists a wide spectrum of available design approaches and models, therefore this uncertainty is likely much more widespread than considered in this work. The novelty of the work lies in the application of spatially-varied CPT data in combination with transformation and model choice uncertainties to lateral SSI of monopiles, and in the analysis of how statistical properties of the CPT profiles influence the nature of the responses obtained. The influence of these on the resulting load-displacement, moment-rotation, and system natural frequency predictions, and the corresponding impact is discussed.

2.0 Geotechnical uncertainty and soil modelling:

Geotechnical uncertainties occur in two different variants, (i) aleatory or natural variability, and (ii) epistemic or knowledge uncertainty [31]. Aleatory uncertainty refers to the spatial and temporal variation inherent to the soil in question [32]. This uncertainty is a fundamental property of the soil and though it can be measured more accurately, via additional site investigation or laboratory tests, it cannot be eliminated [33]. Epistemic uncertainty refers to uncertainty brought about by a lack of understanding. Significant sources of knowledge uncertainty exist in geotechnics including (i) model uncertainty, (ii) measurement uncertainty, (iii) transformation uncertainty, and (iv) stratification uncertainty, see Figure 1. While

epistemic uncertainty can be substantial, it can, by definition, be reduced through knowledge gain. In this paper, the effects of both spatial variation and model uncertainties are examined [34–36]. The following sections provide details on how these uncertainties are incorporated in the present study.

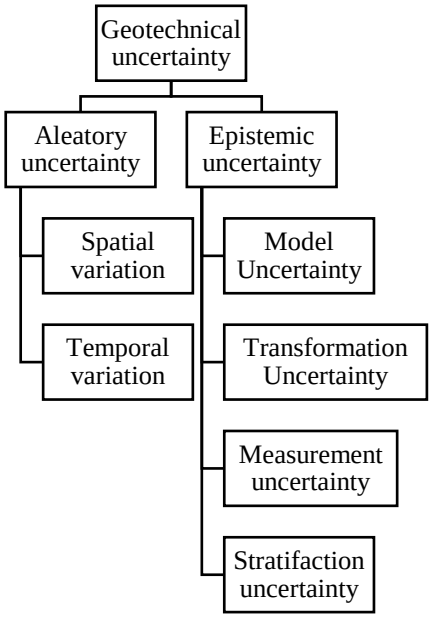

Figure 1 Sources of geotechnical uncertainty

2.1 Stochastic ground model:

Soil as a naturally variable material has properties that vary with both time and space. Traditionally, soil variability was accounted for in design by dividing soil into discrete layers and assigning representative conservative fixed parameter values to each layer. While such an approach has the benefit of simplicity, it masks the true behaviour of the soil, which may lead to unforeseen settlement/structural responses upon completion. Furthermore, it promotes the use of excess materials leading to greater expenditure and carbon emissions. By utilising stochastic ground models, all of the data from a soil layer can be incorporated allowing for more realistic measures of variation across layers and thus can be used to design safe, reliable systems, which are fit for purpose but not overly-conservative.

In this paper, stochastic CPT profiles are developed using the random field approach [37–39], to describe the spatial variability of soil strength. For variables that can be described using normal or log-normal distributions, three parameters are necessary to define the random field of a property, namely the mean, standard deviation and scale of fluctuation (θ), where the θ represents the average distance over which soil properties are significantly correlated. This can also be thought of as the average depth between successive zones of high or low strength. This is a measurable property of a soil that can be obtained either by curve fitting an autocorrelation function to the correlation structure of a detrended CPT [22,27,39] or by using Vanmarcke's method [40] . Scales of Fluctuation should be checked for each layer as they will change as the material changes. The procedure for generating stochastic CPT profiles using known point statistics is outlined below.

Once a layer's θ is known, a correlation matrix can be developed using a correlation function. Numerous correlation functions exist but the Markov correlation structure is the most commonly used and is adopted in this paper, see Equation 1.

$$\rho(\tau_j) = \exp\left(\frac{-2|\tau_j|}{\theta}\right) \quad [1]$$

where $j = 0,1,\ldots, n-1$ with n being the number of data points, $\tau_j = j\Delta\tau$ is the lag distance between the two points in question, ρ is the correlation matrix and θ is the scale of fluctuation. The correlation matrix is positive definite and so can be decomposed into upper ($\mathbf{L^T}$) and lower ($\mathbf{L}$) triangular forms using Cholesky decomposition, see Equation 2.

$$\boldsymbol{\rho} = \boldsymbol{LL^T} \quad [2]$$

A spatially correlated normal random field, **G**, can then be obtained through multiplying the lower triangular matrix with **U**, a matrix of independent normal random numbers with zero mean and unit standard deviation, see Equation 3.

$$\boldsymbol{G} = \boldsymbol{LU} \quad [3]$$

To generate stochastic CPT profiles using the correlated normal random field **G**, the random field needs to be scaled to the correct dimension using the relevant point statistics (mean and standard deviation, in this case), see Equation 4.

$$\boldsymbol{q_c} = \mu + \sigma \boldsymbol{G} \quad [4]$$

where μ is the mean CPT tip strength (q_c) value described at a depth *z* using Equation 5, and σ is the standard deviation at the same depth.

$$\mu(z) = a_i + b_i z \quad [5]$$

where a_i is the value of the mean trend at the beginning of the *ith* layer, b_i is the slope of that trend in the same layer, and *z* is the depth into the stratum.

In this study, two different mean profiles have been considered: (i) a profile with a constant value of 15 MPa with depth to simulate an over-consolidated deposit, and (ii) a profile that linearly increases with depth from a value of 0 MPa at the ground surface to a value of 30 MPa at 30m below ground level (bgl) to simulate a normally-consolidated deposit, see Figure 2 and Figure 3. As the foundation being considered in the present study extends to 30 m bgl, the mean of both soil profiles is the same when averaged over the layer in question. To interrogate how a soil's underlying spatial variability affects the response of a wind turbine system, a series of spatially correlated CPT profiles were generated about both of these fixed mean profiles considering θ of 0.2 m, 0.4 m, 0.7 m, 1.0 m and 1.3m, see Figure 4, and coefficients of variation (CoV) of 0.05, 0.1, 0.15, 0.2 and 0.3 respectively.

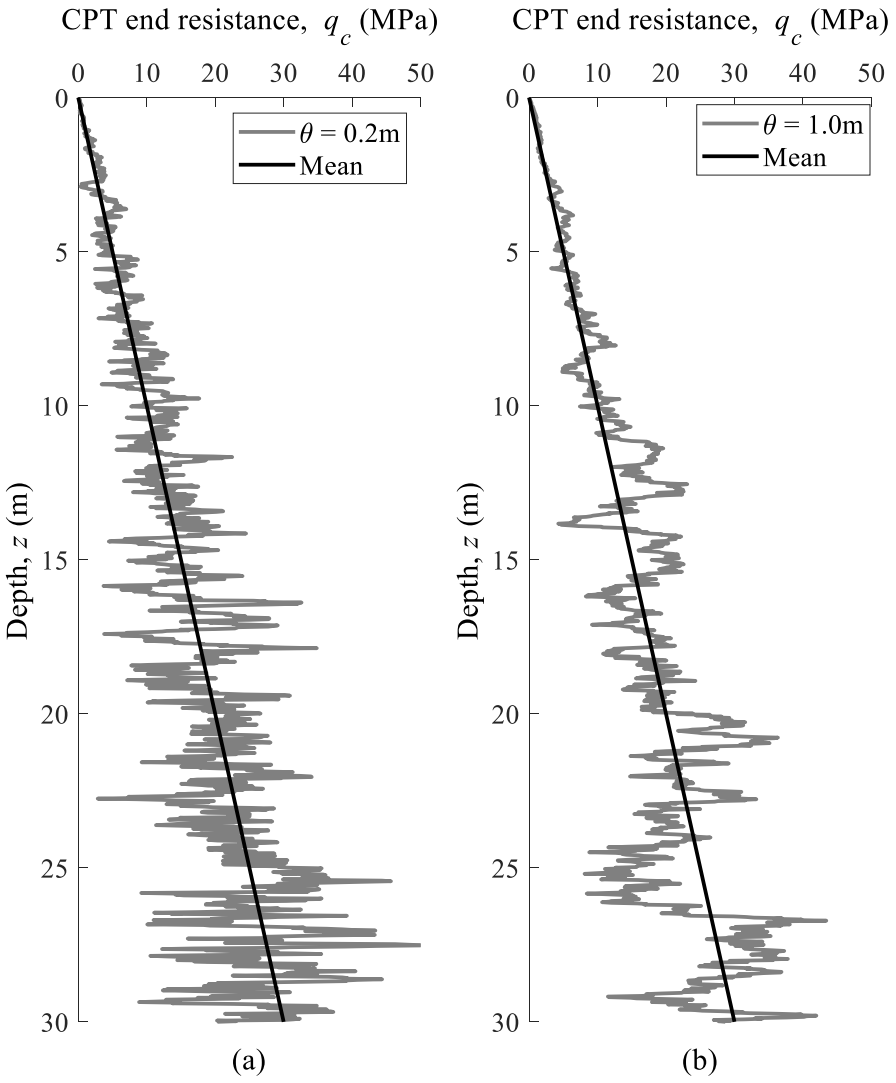

Figure 2 Mean profile considered for linearly increasing strength with depth case (normal consolidation), with randomly generated CPTs, for CoV = 0.3, where in (a) θ = 0.2 m, while in (b) θ =1.0 m.

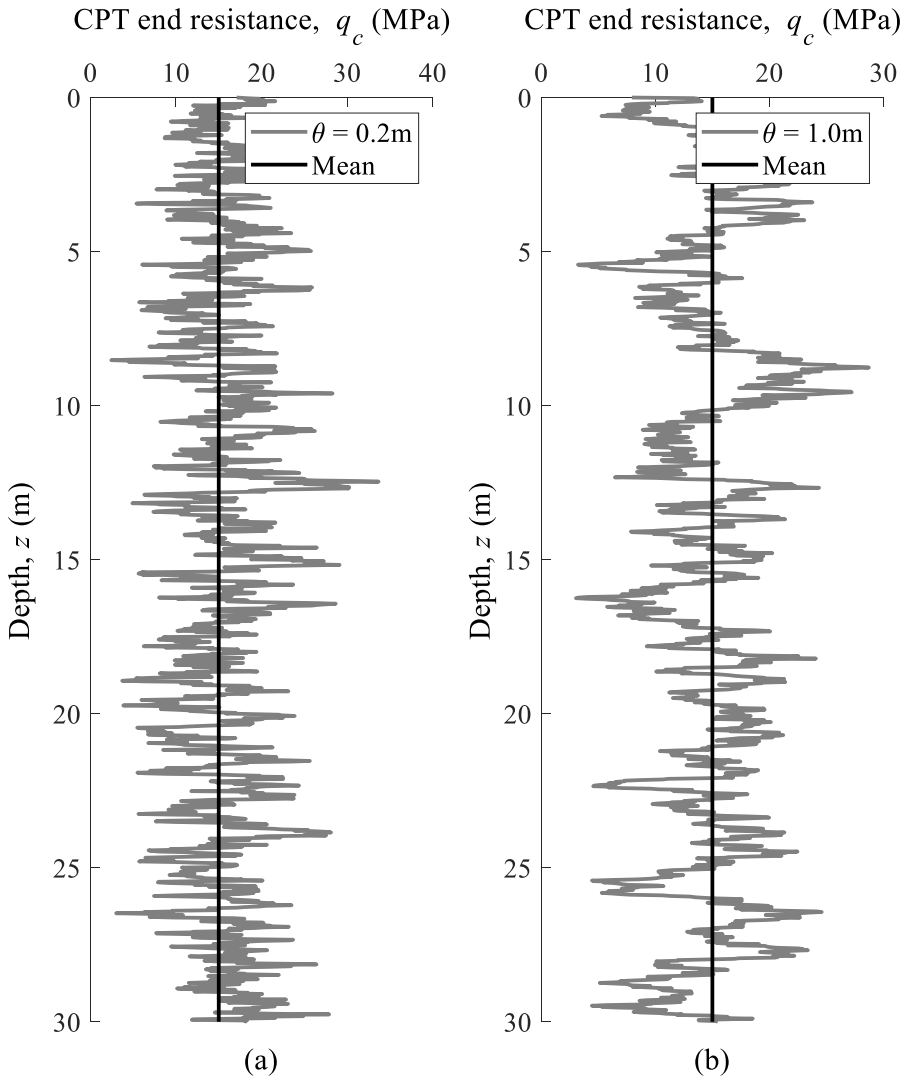

Figure 3 Mean profile considered for uniform strength with depth case (over-consolidation), with randomly generated CPTs, for CoV = 0.3, where in (a) θ = 0.2 m, while in (b) θ =1.0 m.

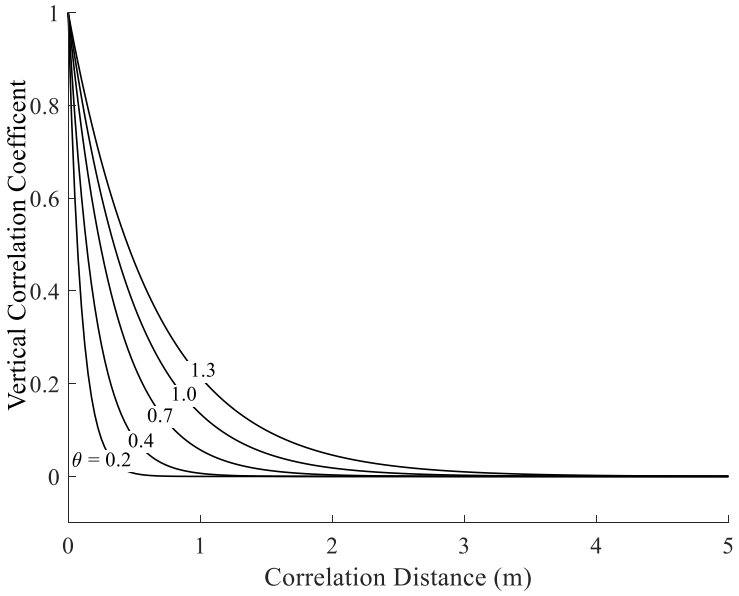

Figure 4 The correlation distances of the different scales of fluctuation considered in this study (θ = 0.2 to 1.3)

2.2 Model transformation error in small-strain shear modulus:

For dynamically-sensitive structures such as wind turbines, predicting operational soil stiffness is critical as an over or under-prediction of the system frequency can affect stability and shorten the operational life of the structure through fatigue [41]. During operation, OWTs typically remain within the small-strain elastic region for SSI, as a result the small-strain shear modulus (G_0) governs the soil-structure response. This is a difficult parameter to measure accurately without in-situ geophysical testing, which can be difficult to perform offshore. To overcome this, numerous researchers [25,42,43] have suggested correlations between G_0 and q_c. Equation 6 presents a simple expression, known as the rigidity index, which varies depending on the soil type, age, and stress history of the deposit in question. Even within a homogenous soil layer there can be quite a spread in this coefficient. To account for this model transformation error in the present study, n was assumed to be a random variable with a mean

value of 6 (as recommended for a dense sand) with a standard deviation of 1. A truncated normal distribution was assumed with a minimum value of 5 and a maximum boundary of 8 [44]. It should be noted that a wide variety of expressions exist that correlate G_0 with q_c and the approach adopted in the present work is not intended to be exhaustive. Instead, the purpose is to demonstrate the influence of variability when a certain case is considered.

$$G_0 = nq_c \quad [6]$$

2.3 Coefficient of subgrade reaction:

Another source of uncertainty in small-strain dynamic modelling of SSI is the implementation of subgrade reaction models to characterise the coupling stiffness between soil and structural elements through beams supported on discrete Winkler springs [10]. There exists many formulations for the coefficient of subgrade reaction, k_s [11,23], each with inherent underlying assumptions. Two common models used for this were developed by Biot [45] and Vesic [46], as shown in Equations 7 and 8.

$$k_s = \frac{0.95E_0}{D(1-{v_s}^2)}\left[\frac{E_0 D^4}{EI(1-{v_s}^2)}\right]^{0.108} \quad [7]$$

$$k_s = \frac{0.65E_0}{D(1-{v_s}^2)}\left[\frac{E_0 D^4}{EI}\right]^{1/12} \quad [8]$$

where E_0 is the small-strain Young's modulus of soil, D is the pile diameter, v_s is the small-strain Poisson ratio, E is the Young's modulus of the pile material, and I is the second moment of area of the pile in bending. Equation 7 is an empirical expression, derived from a solution to an infinite beam problem with a concentrated load resting on a 3-D elastic soil continuum where the maximum moments in the infinite beam are equated. Equation 8 is derived from a similar problem where the maximum displacements of the infinite beam are equated.

The differences in Equations 7 and 8 are due to differences in the assumptions underlying their formulation. This presents a natural issue to designers who must choose a model to characterise SSI coupling stiffness. For identical pile and soil mechanical properties, the adoption of Equations 7 and 8 can lead to a significant difference in the predicted dynamic response of SSI systems. Note also that these are just two examples of these types of expressions. A range of methods exist that are not considered in the present work. Interested readers are referred to the works of Gazetas [16,47] for more information.

3.0 Structural modelling:

3.1 Wind turbine model:

The wind turbine model employed in this paper is programmed in MATLAB using one-dimensional (1-D) finite elements and represents typical properties of a 3.6 MW offshore wind turbine [48–51]. The foundation structural and geometrical properties were derived (designed) based on preliminary sizing estimates provided in Sørensen and Ibsen [52] and the application of the design approach presented in Arany et al. [16]. Monopiles supporting OWTs have typical penetration depths of L = 15 - 30m, wall thicknesses of 50 - 120 mm, and pile diameters of D = 4 - 6 m. These parameters are relevant for monopiles supporting OWTs with rated capacities in the range of 2 - 5 MW, located in water depths ranging between 10 - 25 m. The foundation properties for the present system were tailored to the example case in this paper using a simplified design load basis derived assuming a simple wind/wave load scheme [22,53,54]. It was assumed that the applied wind and wave forces for design are those experienced by the OWT under normal operating conditions, i.e. a wind speed of 12 m/s [48,50,51]. Furthermore, the wind and wave forces are assumed (i) to depend on wind velocity and the geometry of the structure, (ii) to be co-directional, and (iii) to depend on simplified aero- and hydrodynamic

factors. More detail on the derivation of the applied loads for sizing systems of this nature is available in Prendergast et al. [22].

The Critical Pile Length Criterion, defined in Arany et al. [16], was used to calculate the required embedded length, resulting in L=30m. A monopile wall thickness of 0.08 m was adopted for compliance against the applied loads and moments from the simplified environmental load calculations, see section 3.2. The monopile supports a 70 m high tower, which is assumed to taper from a base width of 5 m to a top width of 3.5 m, with a wall thickness of 0.045 m. The tower height is chosen so that the hub height above mean sea level equates to 85 m, approximately in line with the expected hub height [49–51], see Figure 5. The nacelle/rotor mass assembly was chosen to be 230,000 kg, broadly in line with the reported mass for systems of this size [49–51]. The geometrical properties of the tower were tailored to ensure that the entire system frequency of the structure resided between the excitation frequency bands of the rotating blade system, reported as having a rotational velocity varying between 5-13 revolutions per minute (RPM) [49,50]. This results in a 1P (rotor) excitation band of approximately 0.08 Hz – 0.22 Hz, and a 3P (blade passing) excitation band of 0.25 Hz – 0.65 Hz. Details on calculating the system natural frequency of the model are provided in section 3.3. The main model properties are summarised in Table 1, and Figure 5 shows a schematic of the modelled system.

Table 1 Wind turbine assumed structural properties

Element	**Value**	**Unit**
Tower length	70	m
Tower Young's modulus	210	GPa
Tower diameter	5 – 3.5	m
Tower wall thickness	0.045	m
Nacelle/Rotor mass	230	tonnes
Monopile length	75	m
Embedded length	30	m
Monopile Young's modulus	200	GPa
Monopile diameter	6	m
Monopile wall thickness	0.08	m

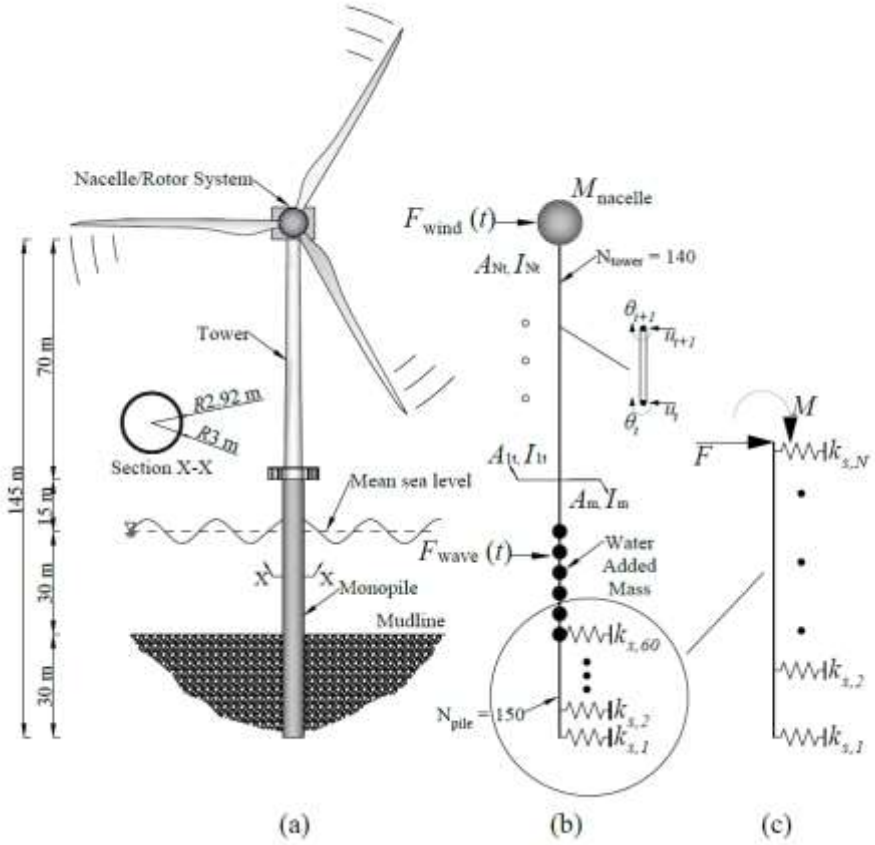

Figure 5 OWT model. (a) schematic, (b) numerical model of full system, (c) numerical model of foundation

3.2 Monotonic lateral load (*p-y*) model:

In order to investigate the effect of geotechnical uncertainty (in CPT data) on the static response characteristics of monopiles, a nonlinear lateral pile-soil interaction model is developed as described in this section. To ensure structural safety and satisfy Serviceability Limit State (SLS) requirements, monopile properties should be selected that limit pile head (mudline) deflection and rotation to prescribed allowable values. Pile head (mudline) rotation should be limited to 0.25° over the service lifetime of the OWT, while an additional 0.25° of tilt is permitted during installation. An allowable cumulative pile head displacement of 0.2 m over the entire service life is permitted at the mudline [16].

To investigate the effect of varying soil properties on the load-displacement and moment-rotation of the monopile, the *p-y* method is employed, as described herein. The *p-y* method assumes that the pile behaves as an elastic beam supported by a series of uncoupled nonlinear springs representing the soil medium. The beam sections consist of four degree of freedom (4-DOF) Euler-Bernoulli beam elements [55] where each node is connected to a lateral spring. In cohesionless soils, the American Petroleum Institute's (API) hyperbolic tangent function, as recommended in the Det Norske Veritas (DNV) design standards [19] is commonly used to characterise the *p-y* behaviour. The API uses the sand's angle of internal friction, ϕ', to construct a hyperbolic relationship between *p* and *y*. However, the API method has come under heavy scrutiny due to the sensitivity associated with extracting accurate ϕ' values from stratigraphic data. Additionally the API method was originally derived from experimental results on slender piles (*L/D* = 34) [56,57], calling into question its suitability when used for systems with larger diameters [5,58–60]. A function developed by Suryasentana and Lehane [61] using 3D finite element analyses of monopiles (diameters up to 5 m) describes the nonlinear relationship between *p* and *y* as a function of CPT tip resistance (q_c), to directly incorporate measured soil strength. This addresses the drawbacks associated with the use of ϕ' values, which incur parameter transformation errors, and additionally has been shown to be accurate for large-diameter offshore monopiles [62].

The numerical monopile model was developed in MATLAB employing Euler-Bernoulli beams supported on nonlinear Winkler springs, where the properties of the springs were derived using the CPT-based *p-y* model from Suryasentana and Lehane [61,62]. Figure 6 shows the configuration of the monopile model and demonstrates how a discretised CPT profile is used to characterise each discrete *p-y* spring. The spring stiffness for a given pile

displacement is defined as the secant modulus of the respective *p-y* curve and the soil's unit weight γ is assumed to be $20kN/m^3$ for all cases considered in this paper.

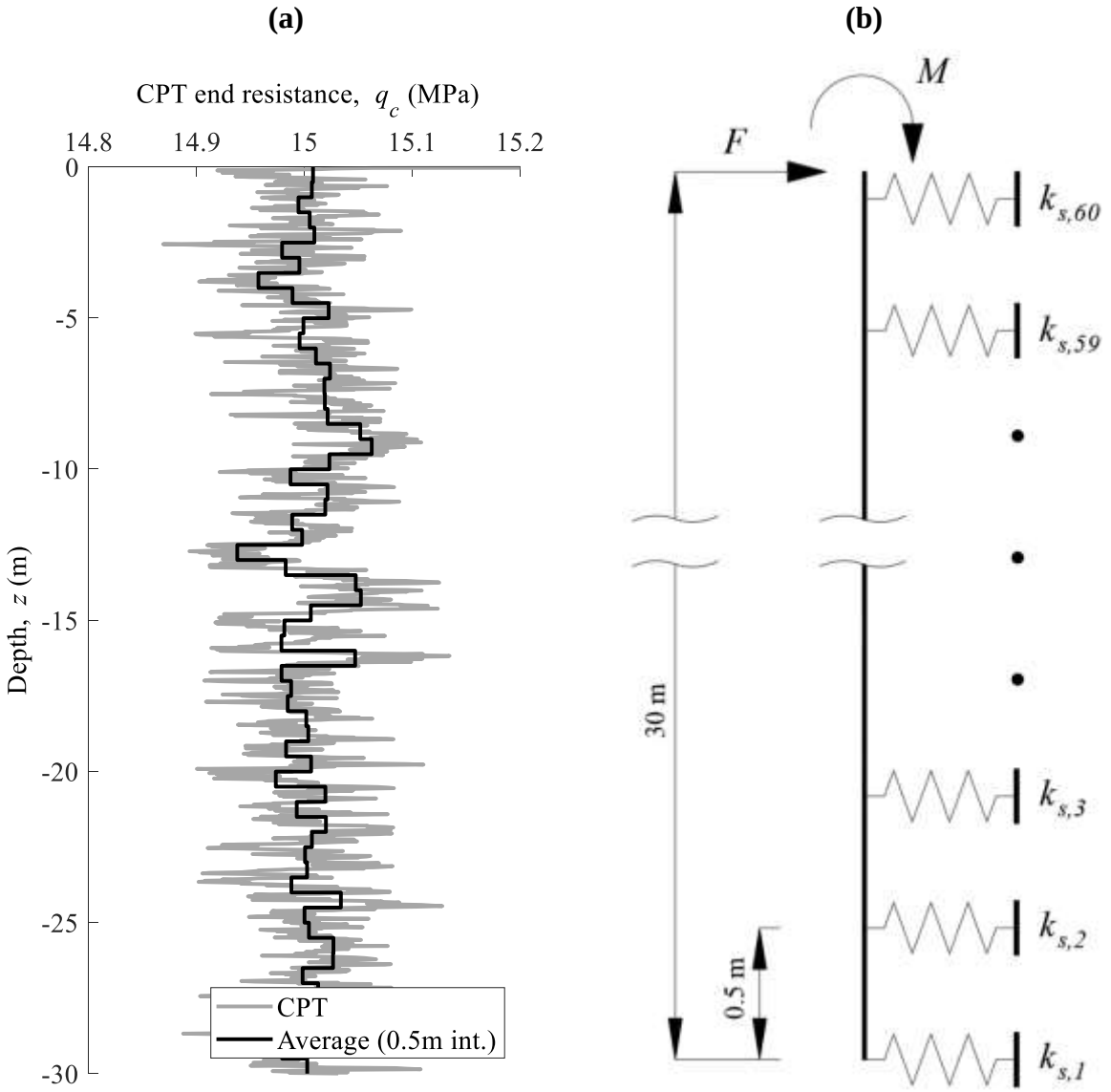

Figure 6 Example of discretisation process for CPT profile into model (a) CPT profile, (b) Winkler-based (p-y) model

Equation 9 shows the *p-y* model employed.

$$\frac{p}{\gamma x D} = 2.4\left(\frac{q_{c,avg}}{\gamma z}\right)^{0.67}\left(\frac{z}{D}\right)^{0.75} \times \left\{1 - \exp\left(-6.2\left(\frac{z}{D}\right)^{-1.2}\left(\frac{y}{D}\right)^{0.89}\right)\right\} \quad [9]$$

where p is the soil reaction at a given spring depth (kN/m), γ is the bulk unit weight of the soil (kN/m^3), z is the spring depth (m), D is the pile diameter (m), y is the lateral deflection of the spring (m) and $q_{c,avg}$ is the CPT end resistance value averaged over the discretised spring length (kPa). The initial stiffness modulus of each spring is specified in Equation 10 [62].

$$E_{s0} = \left(\frac{dp}{dy}\right)_{y=0} \approx 4G_0(1+v_0) \approx 4.5G_0 \quad [10]$$

where G_0 is the initial (maximum) shear modulus of the soil and v_0 is the Poisson ratio (typically 0.1 to 0.2). The initial shear modulus can be readily extracted from q_c values through the simple expression $G_0 \approx 6q_c$ [44].

The computational procedure for the analysis is as follows: an initial calculation of monopile displacements is computed utilising spring stiffness values determined from Equation 10. These displacements are subsequently used to calculate a new operating secant stiffness for each spring using Equation 9 ($E_{si} = p/y$, where E_{si} is the secant stiffness for a given iteration). The system matrices are re-formulated and the displacements corresponding to the new stiffness values are obtained. This process is iterated until a predefined tolerance is met and equilibrium is achieved with the external loads applied. The MATLAB model was validated against commercially available software and good agreement was observed.

3.3 Dynamic model:

The dynamic OWT is modelled as a system of mathematical equations using the stiffness matrix method. The tower and monopile are modelled using four degree-of-freedom Euler-Bernoulli (4-DOF) beam elements, with consistent mass and stiffness matrices available in Kwon and Bang [55]. Each beam element is 0.5 m in length. The soil within the embedded portion of the pile is incorporated as an added mass, assuming the bulk density of sand as 20 kN/m^3. This is considered as an equivalent amount of steel by increasing the effective cross-

sectional area of the pile (but not the second moment of area so as not to add additional stiffness). Hydrodynamic and internal water added mass are included in the form of point masses added to the lateral degrees of freedom of the monopile for the portion of the pile extending above the mudline but below the mean sea level. Seawater density of 1025 kg/m^3 and a coefficient of added mass C_a=2 are assumed, 1 for external mass and 1 for internal mass [54,63]. Finally, the rotor/nacelle is considered as a lumped mass at the top of the tower, by adding a point mass to the lateral degree of freedom at this location. The SSI is incorporated using a beam-Winkler framework [10,11,23] whereby the soil-pile interaction is considered as a distributed system of linear springs in contact with the pile beam elements, as described previously. The spring stiffnesses are obtained by application of subgrade reaction formulae, which couple soil and pile properties together [24,45,46]. The coupling formulae used in this paper are discussed previously in section 2.3. The individual spring stiffnesses are derived from the stochastic ground model CPT data using the small-strain shear transformation discussed previously (rigidity index). Table 1 outlines the model properties and Figure 5 shows a schematic of the turbine modelled.

The natural system (undamped) frequencies of the OWT for a given set of ground stiffness values are obtained by solving the Eigenproblem shown in Equation 11.

$$([\mathbf{M^{-1}K}] - \boldsymbol{\lambda}[\mathbf{I}])\{\mathbf{A}\} = \{\mathbf{0}\} \quad [11]$$

where $[\mathbf{I}]$ is the identity matrix, $([\mathbf{M^{-1}K}] - \boldsymbol{\lambda}[\mathbf{I}])$ is the characteristic matrix, $\lambda = \omega^2$ are the eigenvalues, and $\{\mathbf{A}\}$ are the eigenvectors. The eigenvalues (natural frequencies) are obtained by solving the characteristic equation using MATLAB.

The procedure to obtain distributions of system natural frequencies arising from the stochastic model inputs is demonstrated in the flow chart in Figure 7.

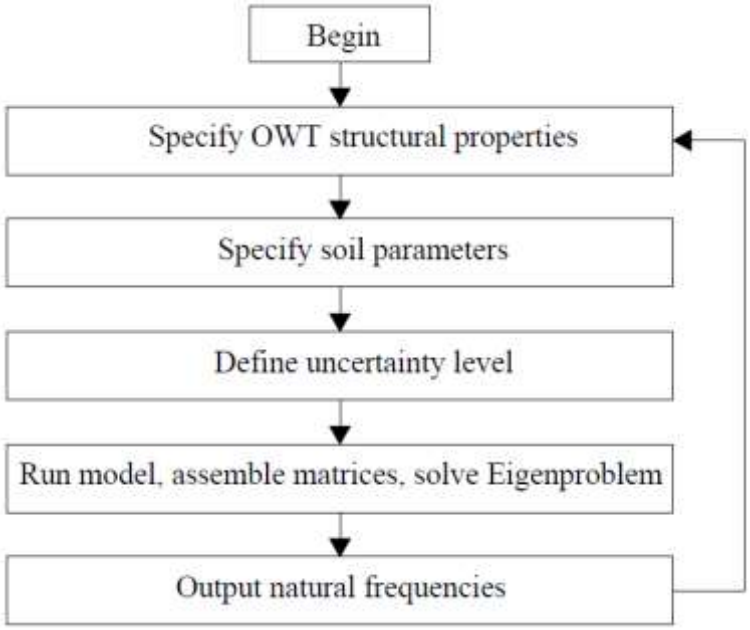

Figure 7 Flow chart for extraction of OWT frequency distribution

4.0 Analysis and results:

This section contains the results of considering the influence of geotechnical uncertainty as described in the previous subsections, on design pile head load-displacement, moment-rotation, and system natural frequency estimations for the example OWT considered in this paper.

4.1 Monotonic monopile response

The pile lateral load model described in section 3.2 is implemented in this section in tandem with the stochastic CPT ground model to ascertain the influence of geotechnical uncertainty on the predicted response features of the monopile foundation. A design lateral load and moment of 1155 kN and 93225 kNm, respectively are applied at the mudline, as derived using the simplified environmental load calculations discussed previously [22,54]. The resulting pile head (mudline) deflections and rotations with all considered scales of fluctuation for both the stochastic linear and uniform CPT profiles are presented in Table 2 and Table 3

respectively. For both the linearly increasing (normally-consolidated) and uniform strength with depth (over-consolidated) cases, a mean CPT profile, and upper bound and lower bound profiles taken at two standard deviations either side of the mean were considered, to investigate the influence of variability on the response, see Figure 8.

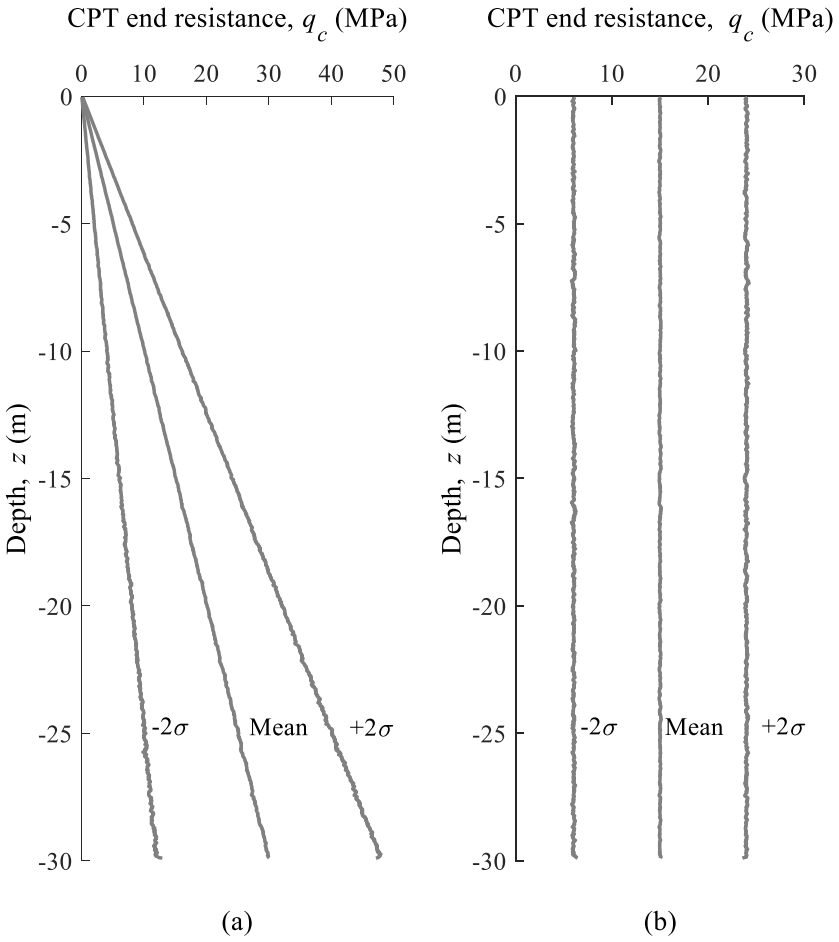

Figure 8 CPT profiles used in monotonic calculations for θ = 0.2, (a) linearly increasing mean ± 2σ, (b) uniform mean ± 2σ

It was observed that, for an increase in θ, there was a negligible change in pile head (mudline) deflection, most likely as a result of the profile being averaged out in the discretisation process for formulating the individual Winkler springs. This is likely to be the case until the θ is far larger than the spring spacing. Both the pile head displacements and rotations for all stochastic soil profiles are well within the SLS limits defined previously (0.25°

rotation and 0.2 m displacement at mudline). It should be noted that this is a fundamental SLS check and only applies the required considerations necessary for preliminary analysis, plastic accumulation in rotation was not considered in the models.

Table 2 Results of applying the linear CPT profile to the lateral pile analysis

θ	**Mean**		**-2σ**		**+2σ**	
	δ **(m)**	θ_p **(°)**	δ **(m)**	θ_p **(°)**	δ **(m)**	θ_p **(°)**
0.2	0.02155	0.10415	0.03741	0.15173	0.01678	0.08955
0.4	0.02154	0.10411	0.03726	0.15120	0.01678	0.08956
0.7	0.02155	0.10413	0.03722	0.15100	0.01679	0.08959
1.0	0.02154	0.10411	0.03711	0.15058	0.01679	0.08960
1.3	0.02155	0.10413	0.03708	0.15037	0.01680	0.08963

Table 3 Results of applying the uniform CPT profile to the lateral pile analysis

θ	**Mean**		**-2σ**		**+2σ**	
	δ **(m)**	θ_p **(°)**	δ **(m)**	θ_p **(°)**	δ **(m)**	θ_p **(°)**
0.2	0.01164	0.07641	0.02028	0.10909	0.00904	0.06621
0.4	0.01163	0.07639	0.02024	0.10890	0.00904	0.06621
0.7	0.01163	0.07640	0.02021	0.10880	0.00904	0.06623
1.0	0.01164	0.07641	0.02019	0.10859	0.00904	0.06624
1.3	0.01165	0.07644	0.02019	0.10858	0.00905	0.06627

Figure 9 shows the load-displacement and moment-rotation response curves for the pile head (at mudline) corresponding to the CPT profiles with θ = 0.2. The loads and moments are incrementally applied up to and beyond the design values discussed previously and shown on each plot. The results for the mean profile and two standard deviations each side of the mean are shown for both linear and uniform CPT data, as in Table 2 and Table 3. It can be observed that for a given profile (mean, -2σ, +2σ) the corresponding displacements are larger for the linearly increasing CPT profile when compared to the uniform profile, due to the correspondingly lower CPT end resistance values near the mudline for this profile. In Figure 9(a), the model implementing upper-bound uniform profile experiences ≈ 21% lower pile head displacement at the design load than that using the mean profile, whilst the model implementing

the lower-bound profile experiences ≈ 67% higher pile head displacements. Similarly for the linearly increasing profile, pile head displacement at the design applied load is ≈ 21% lower for the model implementing the upper-bound profile when compared to the equivalent mean profile, and ≈ 71% higher for the model implementing the lower-bound profile. In Figure 9(b), the pile head rotation at the design applied moment is ≈ 12% lower for the model implementing the upper-bound uniform profile and ≈ 39% higher for the model implementing the lower-bound uniform profile when compared to the equivalent mean profile. Similarly, the pile head rotation at the design applied moment is ≈ 13% lower for the model implementing the upper-bound linearly increasing profile and ≈ 44% higher for that implementing the lower-bound linearly increasing profile when compared to the equivalent mean profile. This analysis highlights that variation in the profile resulting in a softer, less stiff material has an exacerbated effect on the resulting deflection and rotations due to the nonlinear pile-soil interaction, and suggests that it is important to be able to accurately estimate the acting strength to ensure compliance against design loading.

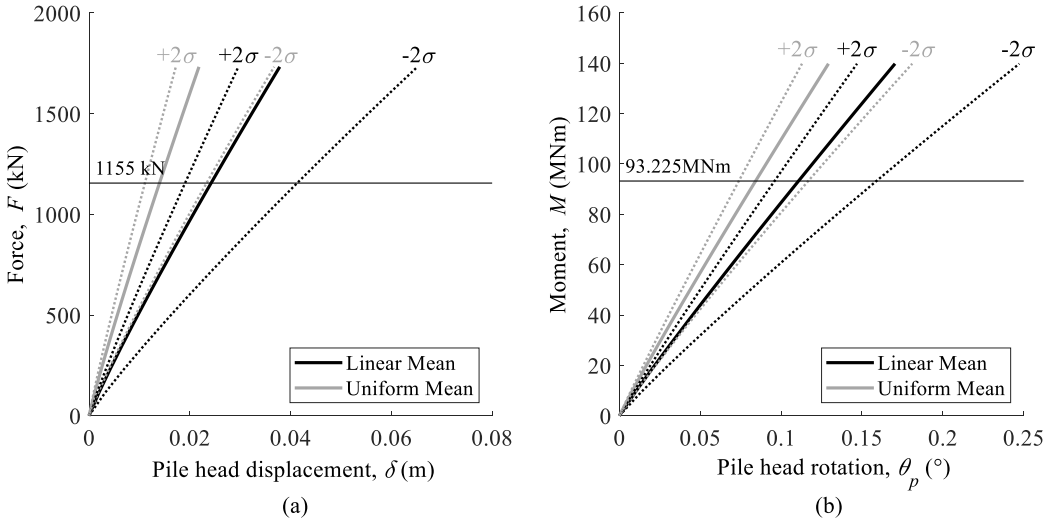

Figure 9 Pile monotonic response analysis. (a) load-displacement, (b) moment-rotation

4.2 System natural frequency response

To ensure safe turbine operation and avoid resonance issues, OWTs need to be designed so that the natural frequency of the system resides away from excitation bands. For those founded on monopiles, this typically falls into the soft-stiff zone (between the rotor and blade passing frequencies). If the design natural frequency is too low the system risks interacting with the 1P frequency generated by the rotor, whilst if the structure's natural frequency is too high it could potentially interact with the 3P frequency generated by the turbine blades. In this study, the design system frequency was assessed probabilistically using 10,000 random CPT profiles that were generated using the procedure described in Section 2, before being inputted into the models described in Sections 3.1 and 3.3. By analysing the frequency response probabilistically, it is possible to check how accurate the design frequency is likely to be and obtain a measure of the relative safety offered by that choice given the uncertainties present in the system.

The system natural design frequency was checked for soil profiles where the strength linearly increases with depth (the most likely case) and for soil profiles where the soil strength remains constant with depth. A range of likely scales of fluctuation {0.2 m, 0.4 m, 0.7 m, 1.0 m and 1.3 m} and CoVs {0.05, 0.1, 0.15, 0.2 and 0.3} were considered. The rigidity index described in Equation 6 was used to generate small-strain shear stiffness profiles from the CPT data, and both Biot and Vesic subgrade reaction models (Eqs. 7 and 8) were considered. Note, it should be recognised that a significant number of models exist that can transform CPT data to small-strain stiffness and model the small-strain SSI, so the results in this section are merely to highlight the nature of the possible uncertainties rather than to be an exhaustive analysis of every uncertainty source.

Figure 10 shows how the design natural frequency of the example turbine used in this paper changes based on soil spatial variability for a linearly increasing soil profile using the Biot subgrade model. The plotted percentiles (2.5^{th} and 97.5^{th}) show the dispersion in the predicted natural frequency as both CoV and θ increase. The mean natural frequency prediction is relatively invariant to change in θ and/or CoV which is as expected. At low CoVs, the θ has little to no impact on the predicted frequency but as the CoV increases the effect of the θ becomes more pronounced. This can clearly be seen in Figure 10. To have the same dispersion in frequency that occurs when the CoV = 0.3 and the θ = 0.2, at a θ of 1.3 would require a CoV of only 0.12. To put this into perspective a soil with a CoV of 0.12 would be extremely uncommon in nature with most soils having CoVs between 0.2 and 0.4. This therefore shows the impact of considering soil θ during modelling.

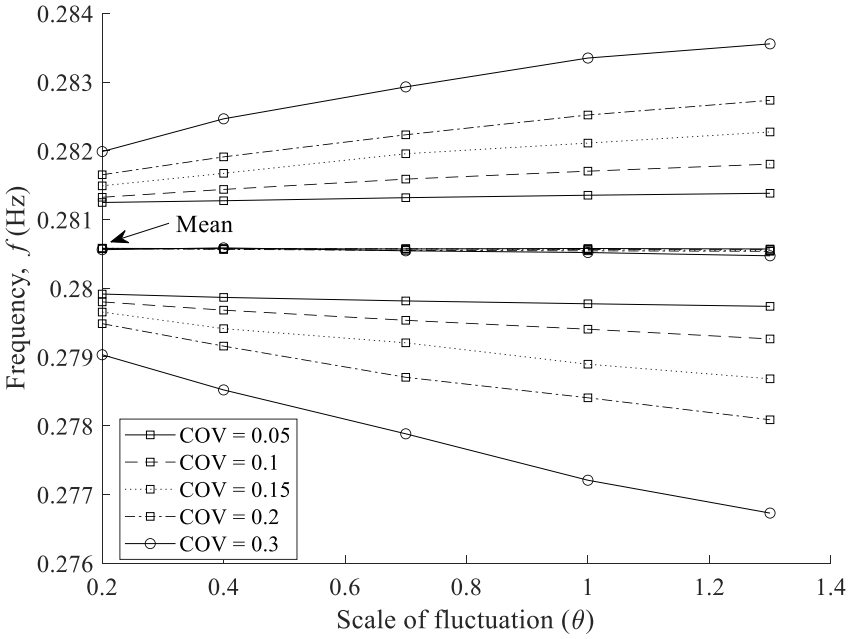

Figure 10 Frequency confidence intervals (α = 0.05) for increasing scale of fluctuation and COV assuming Biot transform and linearly increasing soil strength

Figure 11 also considers a Biot transform for the same CoVs and θ, however this time a uniform soil strength profile with depth is assumed. As a result, the predicted mean natural frequency is significantly higher, even though the average soil strength over the layer is the same. This is because the relatively higher stiffness of near surface soil has a much more pronounced effect on system frequency than the stiffness of the soil at greater depths. Interestingly, even though the mean frequency has increased, the overall range between the 2.5^{th} and 97.5^{th} for uniform soil profile and linearly increasing soil profile is broadly similar and appears not to have been affected by increasing the near surface stiffness.

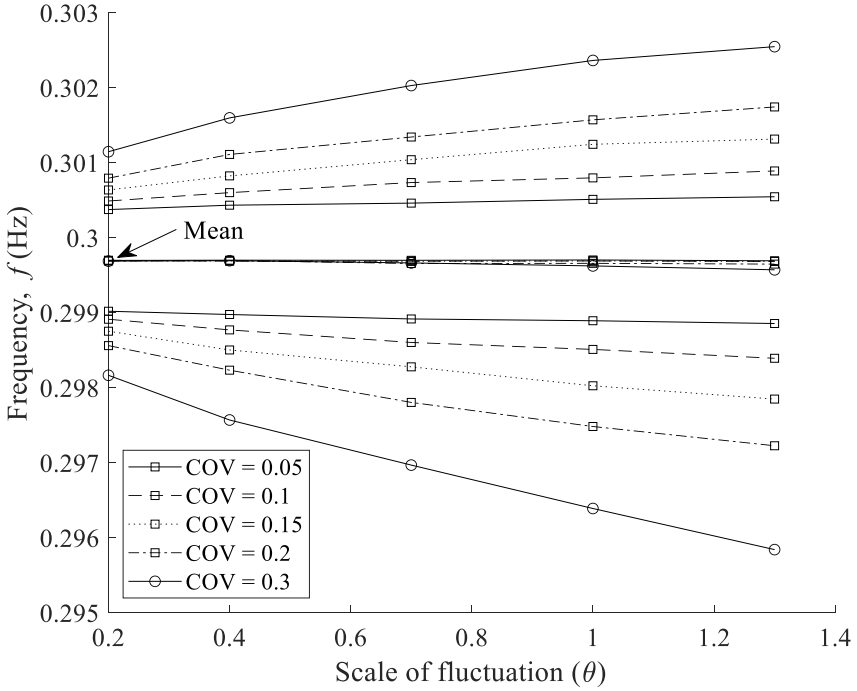

Figure 11 Frequency confidence intervals (α = 0.05) for increasing scale of fluctuation and COV assuming Biot transform and uniform soil strength with depth

Figure 12 and Figure 13 show the same expected frequency variation for the same θ and CoVs as Figure 10 and Figure 11 respectively, however the Vesic subgrade model is employed instead of the Biot model. Figure 14 compares the different models, and shows there is a considerable shift in the mean frequency for both linearly increasing and uniform soil profiles when one uses the Vesic subgrade model instead of the Biot model. The difference is so great in the linearly increasing case that extreme values from the Biot distribution do not overlap with the inter-quartile range of the Vesic distribution and vice-versa. In both cases the mean predicted natural frequency is lower for Vesic than Biot. However, for both linearly increasing and uniform profiles, the range in natural frequency predictions is much higher using Vesic than Biot, see Table 4. As the choice in model significantly alters the position of the mean

frequency it could cause potential interaction effects with the 1P or 3P bands, given it introduces a significant uncertainty as to what the actual system stiffness is.

Changing the subgrade reaction model leads to uncertainty in the location of the mean system frequency, see Figure 14, whilst variation in soil properties leads to a distribution in predicted frequency about that mean. The variation in predicted frequency caused by soil spatial variability is significant, but ultimately being unsure of the location of the mean poses a far bigger problem as it will compound any further variation. As mentioned previously, a variety of models exist for estimating the SSI coupling stiffness, so the potential uncertainties are likely greater than the two cases considered here. The present analysis is limited to two cases for demonstration purposes.

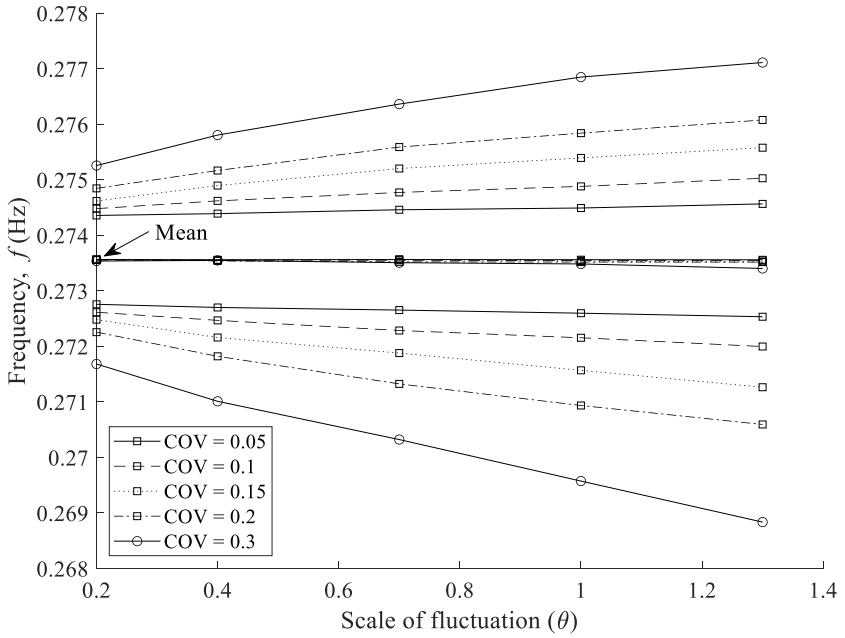

Figure 12 Frequency confidence intervals ($\alpha = 0.05$) for increasing scale of fluctuation and COV assuming Vesic transform and linearly increasing soil strength

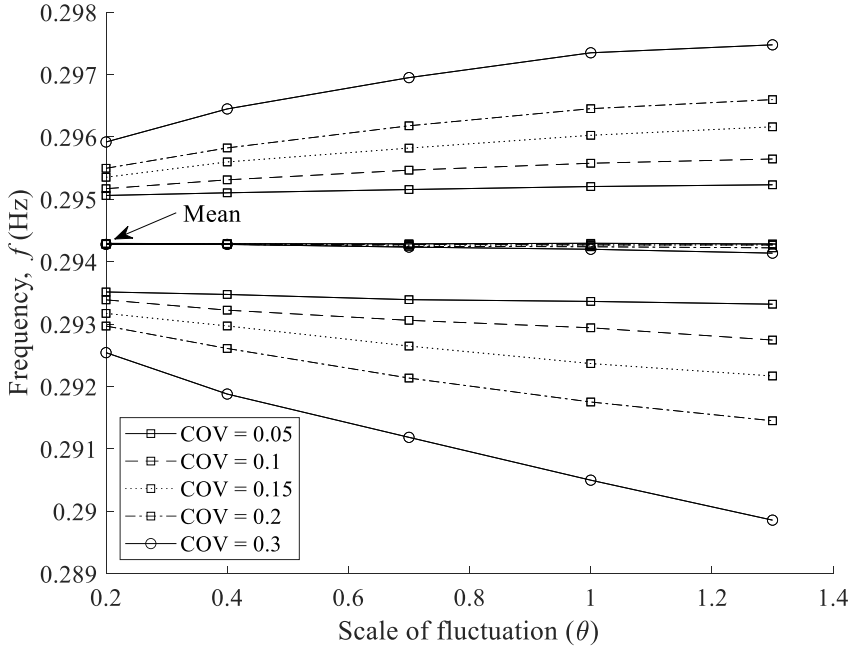

Figure 13 Frequency mean and confidence intervals ($\alpha = 0.05$) for increasing scale of fluctuation and COV, assuming Vesic transform and uniform soil strength with depth

Table 4 Summary statistics

	BIOT		VESIC	
	Linear (Hz)	**Uniform (Hz)**	**Linear (Hz)**	**Uniform (Hz)**
Mean	0.2806	0.2997	0.2736	0.2943
2.5% CI	0.2767	0.2958	0.2688	0.2899
97.5% CI	0.2836	0.3025	0.2771	0.2975
Range	0.0069	0.0067	0.0083	0.0076

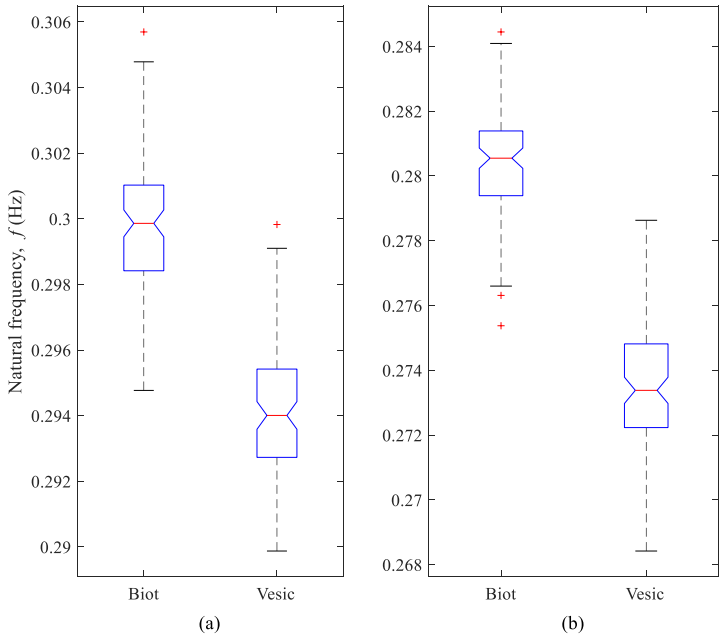

Figure 14 Boxplots comparing the difference between (a) Biot, and (b) Vesic at CoV = 0.3 and θ =1.3 m, where the box represents the inter-quartile range, red-line represents the mean, the notches in the box represent the zone of 95% confidence in the mean, the whiskers indicate extreme values and the crosses outliers.

5.0 Conclusions

In this paper, the influence of geotechnical uncertainty on the predicted monotonic and frequency characteristics of an example monopile-supported OWT is

investigated. Due to the significant recent advances in OWT developments and the move towards installations in less certain geological regions further offshore, this research aims to highlight the potential issues that might be experienced by designers over coming years. Geotechnical uncertainty is considered from the perspective of spatial variability in soil properties (considered as CPT data), parameter transformation issues (using the rigidity index), and subgrade reaction model choice for soil-structure coupling.

In terms of monotonic load-displacement response, changes in the θ of the soil model lead to a negligible change in the resulting pile head deflection. This is likely a result of the averaging process undertaken to discretise the soil profile into separate Winkler springs, which masks any disparity in the profile properties. It should be noted that the process to develop *p-y* models has the potential to lose information from the original soil data, and care should be taken to ensure this data loss is not unconservative.

In terms of predicting the system natural frequency, incorporating θ has a demonstrable effect on this prediction with significantly increased variance found at larger θ. As this is a relatively simple parameter to interpret, the authors recommend that this be checked and considered at highly variable sites. It is of particular importance to do so in difficult soils where finding a suitable natural system frequency that avoids resonance bands may be challenging. Whilst θ has been shown to impact the variation in the predicted natural frequency, the choice of subgrade model represents a much greater uncertainty as it directly impacts the location of the mean natural frequency and hence makes it much more likely that a wind turbine design could have increased risk of resonant interactions. For example, at a θ of 0.2 with a linearly increasing soil strength profile, the Biot model results in a system frequency of approximately 0.2805

Hz, whereas for the same θ and soil profile but using a Vesic model, the system frequency is predicted as approximately 0.2735 Hz. As the θ increases, this discrepancy in system frequency will further increase. Indeed, from the parametric study carried out, the choice of subgrade model displaces the location of the mean by over four standard deviations. It is therefore apparent that the impact of subgrade model choice is substantially larger than the impact of soil spatial variability and small-strain transformation on the reponses. In the absence of further information, it is critical therefore to check multiple subgrade models or other approaches to ensure system reliability.

The Biot model was shown to predict larger system frequencies than the Vesic model, while the Vesic model was observed to have a slightly larger range. Neither model's 95% mean confidence intervals overlapped. This highlights the influence of practitioners' model choice on further analysis and the associated uncertainties. It should be noted that there exists many further expressions than the two models employed in the present work, it would therefore be prudent for designers to use a range of approaches to improve design reliability or confidence.

Whilst accounting for soil spatial variability caused a spread in predicted frequency it seemed to have a less significant effect than that of subgrade model choice. It should be noted however, the impact of soil variability is likely to become more significant in the presence of damaging actions such as scour erosion. This will form the basis of future work on this topic.

The analyses in this paper are limited to uncertainties in CPT resistance, model transformation, and coupling (subgrade) model choice, and it is acknowledged that in reality there exists significantly more sources of uncertainty contributing to this

problem. Moreover, the analyses were conducted on a model incorporating example OWT properties, so the relevance for other types of systems and structures remains a question. The analysis only considered the influence of uncertainties on stiffness, and it should be noted that damping also poses a significant issue to OWTs, and is also potentially highly variable. Damping comes from several sources, and a thorough analysis of the influence of uncertainty in this parameter should be conducted. The results in this paper are potentially only relevant to the conditions studied and further investigation using different methods of soil testing and design situations should be undertaken as part of future work.

Acknowledgements

The second author wishes to acknowledge funding for his PhD under EP/R513283/1 EPSRC Standard Research Studentship (DTP) at the Faculty of Engineering, University of Nottingham.

References

[1] EU. The European Green Deal. Belgium: 2019.

[2] Wind Europe. Offshore wind in Europe - key trends and statistics. 2018. doi:https://doi.org/10.1016/S1471-0846(02)80021-X.

[3] IEA. Offshore Wind Outlook 2019 – International Energy Agency: Special Report. 2019.

[4] UK Government. UK Policy Paper: Offshore Wind Sector Deal. 2019.

[5] Chortis G, Askarinejad A, Prendergast LJ, Li Q, Gavin K. Influence of scour depth and type on p–y curves for monopiles in sand under monotonic lateral loading in a

geotechnical centrifuge. Ocean Eng 2020;197:106838. doi:10.1016/j.oceaneng.2019.106838.

[6] LeBlanc C, Houlsby GT, Byrne BW. Response of stiff piles in sand to long-term cyclic lateral loading. Géotechnique 2010;60:79–90. doi:10.1680/geot.7.00196.

[7] Doherty P, Gavin K. Laterally loaded monopile design for offshore wind farms. Proc ICE - Energy 2012;165:7–17. doi:10.1680/ener.11.00003.

[8] Kampitsis AE, Sapountzakis EJ, Giannakos SK, Gerolymos N a. Seismic soil–pile–structure kinematic and inertial interaction—A new beam approach. Soil Dyn Earthq Eng 2013;55:211–24. doi:10.1016/j.soildyn.2013.09.023.

[9] Yankelevsky DZ, Eisenberger M, Adin MA. Analysis of beams on nonlinear winkler foundation. Comput Struct 1989;31:287–92. doi:https://doi.org/10.1016/0045-7949(89)90232-0.

[10] Winkler E. Theory of elasticity and strength. Dominicus Prague: 1867.

[11] Dutta SC, Roy R. A critical review on idealization and modeling for interaction among soil–foundation–structure system. Comput Struct 2002;80:1579–94. doi:10.1016/S0045-7949(02)00115-3.

[12] Burd HJ, Byrne BW, McAdam RA, Houlsby GT, Martin CM, JAP Beuckelaers W, et al. Design aspects for monopile foundations. TC 209 Work. Found. Des. offshore Wind Struct. ICSMGE, 2017, p. 35–44.

[13] Byrne BW, Burd HJ, Gavin KG, Houlsby GT, Jardine RJ, McAdam RA, et al. PISA: Recent Developments in Offshore Wind Turbine Monopile Design, 2019, p. 350–5. doi:10.1007/978-981-13-2306-5_48.

[14] Zdravković L, Jardine RJ, Taborda DMG, Abadias D, Burd HJ, Byrne BW, et al. Ground characterisation for PISA pile testing and analysis. Géotechnique 2020;70:945–60. doi:10.1680/jgeot.18.PISA.001.

[15] Xue J, Gavin K, Murphy G, Doherty P, Igoe D. Optimization technique to determine the p-y curves of laterally loaded stiff piles in dense sand. Geotech Test J 2016;39:842–54. doi:10.1520/GTJ20140257.

[16] Arany L, Bhattacharya S, Macdonald J, Hogan SJ. Design of monopiles for offshore wind turbines in 10 steps. Soil Dyn Earthq Eng 2017;92:126–52. doi:10.1016/j.soildyn.2016.09.024.

[17] O'Neill M, Murchinson JM. An evaluation of p-y relationships in sands 1983.

[18] API. API RP2A-WSD. 2007.

[19] Det Norske Veritas. DNV Offshore Standard DNV-OS-J101 Design of Offshore Wind Turbine Structures. 2011.

[20] Reese LC, Matlock H. Non-dimensional Solutions for Laterally Loaded Piles with Soil Modulus Assumed Proportional to Depth. Proc. 8th Int. Conf. Soil Mech. Found. Eng., Austin, TX: 1956, p. 1–41.

[21] Prendergast LJ, Gavin K, Doherty P. An investigation into the effect of scour on the natural frequency of an offshore wind turbine. Ocean Eng 2015;101:1–11. doi:10.1016/j.oceaneng.2015.04.017.

[22] Prendergast LJ, Reale C, Gavin K. Probabilistic examination of the change in eigenfrequencies of an offshore wind turbine under progressive scour incorporating soil spatial variability. Mar Struct 2018;57. doi:10.1016/j.marstruc.2017.09.009.

[23] Prendergast LJ, Gavin K. A comparison of initial stiffness formulations for small-strain soil – pile dynamic Winkler modelling. Soil Dyn Earthq Eng 2016;81:27–41. doi:10.1016/j.soildyn.2015.11.006.

[24] Prendergast LJ, Wu WH, Gavin K. Experimental application of FRF-based model updating approach to estimate soil mass and stiffness mobilised under pile impact tests. Soil Dyn Earthq Eng 2019;123:1–15. doi:10.1016/j.soildyn.2019.04.027.

[25] Lunne T, Robertson PK, Powell JJM. Cone Penetration Testing in Geotechnical Practice. Blackie Academic and Professional; 1997.

[26] Mayne P. Interpretation of geotechnical parameters from seismic piezocone tests. 3rd Int Symp Cone Penetration Test 2014:47–73.

[27] Remmers J, Reale C, Pisanò F, Raymackers S, Gavin K. Geotechnical installation design of suction buckets in non-cohesive soils: A reliability-based approach. Ocean Eng 2019;188:106242. doi:10.1016/j.oceaneng.2019.106242.

[28] Wu WH, Prendergast LJ, Gavin K. An iterative method to infer distributed mass and stiffness profiles for use in reference dynamic beam-Winkler models of foundation piles from frequency response functions. J Sound Vib 2018;431:1–19. doi:10.1016/j.jsv.2018.05.049.

[29] Lacasse S, Nadim F, Andersen KH, Knudsen S, Eidsvig UK, Yetginer GL, et al. Reliability of API, NGI, ICP and Fugro Axial Pile Capacity Calculation Methods, Society of Petroleum Engineers (SPE); 2013. doi:10.4043/24063-ms.

[30] Schmoor KA, Achmus M, Foglia A, Wefer M. Reliability of design approaches for axially loaded offshore piles and its consequences with respect to the North Sea. J Rock Mech Geotech Eng 2018;10:1112–21. doi:10.1016/j.jrmge.2018.06.004.

[31] Baecher GB, Christian JT. Reliability and Statistics in Geotechnical Engineering. John Wiley & Sons; 2005.

[32] Reale C, Xue J, Gavin K. Using reliability theory to assess the stability and prolong the design life of existing engineered slopes. Risk Assess. Manag. Geotech. Eng. from Theory to Pract. ASCE Geotech. Spec. Publ. Mem. Late Profr. Wilson H. Tang, 2017, p. Accepted.

[33] Christian JT. Geotechnical engineering reliability: How well do we know what we are doing? J Geotech Geoenvironmental Eng 2004;130:985–1003. doi:10.1061/(ASCE)1090-0241(2004)130:10(985).

[34] Christian JT, Ladd CC, Baecher GB. Reliability Applied to Slope Stability Analysis. J Geotech Eng 1994;120:2180–207. doi:10.1061/(ASCE)0733-9410(1994)120:12(2180).

[35] Phoon K, Kulhawy F. Characterization of geotechnical variability. Can Geotech J 1999;36:612–24.

[36] Whitman R. Organizing and evaluating uncertainty in geotechnical engineering. J Geotech Geoenvironmental Eng 2000;126:583–93. doi:http://dx.doi.org/10.1061/(ASCE)1090-0241(2000)126:7(583).

[37] Fenton G, Vanmarcke E. Simulation of random fields via local average subdivision. J Eng Mech 1990.

[38] Griffiths D, Huang J, Fenton G. Influence of spatial variability on slope reliability using 2-D random fields. J Geotech Geoenvironmental Eng 2009;135:1367–78. doi:http://dx.doi.org/10.1061/(ASCE)GT.1943-5606.0000099.

[39] Lloret-Cabot M, Fenton G, Hicks M. On the estimation of scale of fluctuation in

geostatistics. Georisk Assess Manag Risk Eng Syst Geohazards 2014;8:129–40. doi:10.1080/17499518.2013.871189.

[40] Vanmarcke E. Probabilistic modeling of soil profiles. J Geotech Eng Div 1977;103:1227–46.

[41] Teixeira R, O'Connor A, Nogal M, Krishnan N, Nichols J. Analysis of the design of experiments of offshore wind turbine fatigue reliability design with Kriging surfaces. Procedia Struct. Integr., vol. 5, Elsevier B.V.; 2017, p. 951–8. doi:10.1016/j.prostr.2017.07.132.

[42] Robertson PK. Interpretation of cone penetration tests — a unified approach. Can Geotech J 2009;46:1337–55. doi:10.1139/T09-065.

[43] Schnaid F, Lehane BM, Fahey M. In situ test characterisation of unusual geomaterials. Proc. Int. Conf. Site Characterisation, Porto, Portugal: 2004, p. 49–73.

[44] Prendergast LJ, Hester D, Gavin K, O'Sullivan JJ. An investigation of the changes in the natural frequency of a pile affected by scour. J Sound Vib 2013;332:6685–702. doi:http://dx.doi.org/10.1016/j.jsv.2013.08.020i.

[45] Biot MA. Bending of an infinite beam on an elastic foundation. J Appl Mech 1937;59:A1–7.

[46] Vesic AB. Bending of beams resting on isotropic elastic solid. J Soil Mech Found Eng 1961;87:35–53.

[47] Gazetas G. Seismic response of end-bearing single piles. Int J Soil Dyn Earthq Eng 1984;3:82–93. doi:10.1016/0261-7277(84)90003-2.

[48] Siemens AG. Wind Turbine SWT-3.6-120 Technical Specifications. Hamburg: 2015.

[49] The Wind Power. SWT-3.6-120. Https://WwwThewindpowerNet/Turbine_en_79_siemens_swt-36-120Php 2021. https://www.thewindpower.net/turbine_en_79_siemens_swt-3.6-120.php (accessed May 15, 2021).

[50] ArchiExpo. SWT-3.6-120 Technical Specifications. Siemens Gamesa 2021. https://pdf.archiexpo.com/pdf/siemens-gamesa/swt-36-120/88089-134487.html (accessed May 15, 2021).

[51] Wind Turbine Models. Siemens SWT-3.6-120 Offshore. Wind-Turbine-ModelsCom 2020. https://en.wind-turbine-models.com/turbines/669-siemens-swt-3.6-120-offshore (accessed September 7, 2020).

[52] Peder Hyldal Sørensen S, Bo Ibsen L. Assessment of foundation design for offshore monopiles unprotected against scour. Ocean Eng 2013;63:17–25. doi:10.1016/j.oceaneng.2013.01.016.

[53] Corciulo S. Dynamic Hydro-Mechanical Analysis of Soil-Monopile Interaction in Offshore Wind Turbines. Politecnico Di Milano, 2015.

[54] Corciulo S, Zanoli O, Pisano F. Transient response of offshore wind turbines on monopiles in sand: role of cyclic hydro-mechanical soil behaviour. Comput Geotech 2017;83:221–38. doi:10.1016/j.compgeo.2016.11.010.

[55] Kwon YW, Bang H. The Finite Element Method using MATLAB. Boca Raton, FL: CRC Press, Inc.; 2000.

[56] Reese LC, Cox WR, Koop FD. Analysis of Laterally Loaded Piles in Sand. Proc. Sixth Annu. Offshore Technol. Conf. Houston, TX, Houston, Texas: 1974.

[57] Cox WR, Reese LC, Grubbs BR. Field testing of laterally loaded piles in sand. Proc. Offshore Technol. Conf., Houston, Texas: 1974, p. 4501.

[58] Murchinson JR, O'Niell MW. Evaluation of p-y relationships in cohesionless soil. Anal. Des. pile Found., San Francisco, CA: ASCE; 1984.

[59] Ashford SA, Juirnarongrit T. Evaluation of Pile Diameter Effect on Initial Modulus of Subgrade Reaction. Geotech Geoenvironmental Eng 2003;129:234–42. doi:10.1061/(ASCE)1090-0241(2003)129:3(234).

[60] Yang K, Liang R. Methods for deriving p-y curves from instrumented lateral load tests. Geotech Test J 2007;30:31–8. doi:10.1520/gtj100317.

[61] Suryasentana SK, Lehane BM. Numerical derivation of CPT-based p–y curves for piles in sand. Géotechnique 2014;64:186–94. doi:10.1680/geot.13.p.026.

[62] Suryasentana SK, Lehane BM. Updated CPT-based p – y formulation for laterally loaded piles in cohesionless soil under static loading. Géotechnique 2016;66:445–53. doi:10.1680/jgeot.14.p.156.

[63] Dong RG. Effective mass and damping of submerged structures. 1978.